SCIENCE CHINA
Information Sciences

• RESEARCH PAPER •
Special Focus on Robot Sensing and Dexterous Operation

December 2014, Vol. 57 120201:1–120201:13
doi: 10.1007/s11432-014-5203-8

The relationship between physical human-exoskeleton interaction and dynamic factors: using a learning approach for control applications

TRAN Huu-Toan, CHENG Hong*, LIN XiChuan,
DUONG Mien-Ka & HUANG Rui

Center for Robotics, University of Electronic Science and Technology of China, Chengdu 611731*, China*

Received July 12, 2014; accepted September 15, 2014; published online October 29, 2014

Abstract During a human-exoskeleton collaboration, the interaction torque on exoskeleton resulting from the human cannot be clearly determined and conducted by normal physical models. This is because the torque depends not only on direction and orientation of both human-operator and exoskeleton but also on the physical properties of each operator. In this paper, we present our investigations on the relationship between the interaction torques with the dynamic factors of the human-exoskeleton systems using state-of-the-art learning techniques (nonparametric regression techniques) and provide control applications based on the findings. Experimental data was collected from various human-operators when they were attached to the designed exoskeleton to perform unconstraint motions with and without control. The results showed that regardless of how the experiments were done and which learning method was chosen, the resulting interaction could be best represented by time varying non-linear mappings of the operator's angular position, and the exoskeleton's angular position, velocity, and acceleration during locomotion. This finding has been applied to advanced controls of the lower exoskeletal robots in order to improve their performance while interacting with human.

Keywords physical human-robot interaction, lower limb assistance, lower exoskeleton, non-parametric learning, impedance control

Citation Tran H-T, Cheng H, Lin X C, et al. The relationship between physical human-exoskeleton interaction and dynamic factors: using a learning approach for control applications. Sci China Inf Sci, 2014, 57: 120201(13), doi: 10.1007/s11432-014-5203-8

1 Introduction

Lower exoskeletons are intelligent wearable robots that can be worn by human-operators as orthotic devices for performance assistance and enhancement. The fields of labor intensive industries, military and rehabilitation have witnessed an increasing interest in the practical use of these robotic systems. Although a number of studies related to the design of the lower limb exoskeletons have been developed [1–3], many control-design challenges continue to limit the performance of the systems. One of the difficulties is in estimating the wearer's intended motion from the interaction torques resulting from human on exoskeleton (called resulting physical interaction torque, RPIT) during human-exoskeleton collaboration. For control

* Corresponding author (email: hcheng@uestc.edu.cn)

purposes, these interaction torques play the role of the control command resulting from a human central nerve system, while simultaneously playing the role of the external disturbances necessary to be reduced. The physical interaction torque exerted onto the exoskeleton from the operator is fundamentally affected by the physical properties of each operator's limb segments (that mostly change from person to person and also within one person over time), direction and orientation of the exoskeleton's links during locomotion, and the connection between the operator and exoskeleton. Among these effects on the interaction, practical studies of the relationship between the interaction and measurable motion information will provide promising applications in control-design of the exoskeletal robots. This can be explained as follows. Firstly, a strategy to control these exoskeletons is to estimate the operator's intended motion and compensate for the RPIT. For doing so, almost all practical investigations have involved the estimation of muscle torques from electro-myo-graphical (EMG) information [2,4]. In all these applications, the RPIT were indirectly calculated from the effect of human-operator and in which the setup and calibration of the myo-electric sensors have been the major drawback during working. Besides, the computation of control signals from the drawn EMG signals is not straightforward. Secondly, these interaction torques are usually simplified and represented as a mathematical function of the deviation between the actual angular positions of the operator and exoskeleton [5,6]. However, most of the mathematical model paradigms do not give a sastifying answer to this issue since the RPIT not only depend on the deviation of angular positions, but also on factors relating to the physical properties of a specific wearer as well as how well he/she fits with the machine.

Inspired by the above fundamental issues, the goal of this paper is to investigate the best appropriate relationship between the resulting interaction torque from humans and the dynamic factors related to both the human-operator and exoskeleton, such as angular position, velocity and acceleration of the system. Here, supervised learning technologies [7], from a global method (Gaussian Process Regression) to a local method (Locally Weighted Projection Regression) were used and compared to assure that the findings are significantly reliable. The findings has provided control applications for a lower extremity exoskeleton developed at Pattern Recognition Machine Intelligence Laboratory (PRMI) (Figure 1).

The remainder of this paper is organized as follows; Firstly we discuss how the mapping between the RPIT and dynamic factors is carried out. Subsequently, we generally present the regression techniques utilized in this work. Experimental evaluation is described in the next section. Finally, the control applications of the findings will be briefly presented.

2 Related work

For human performance enhancement, the key issue of exoskeleton control is to drive the robot to work in concert with the operator during locomotion while the combined human-exoskeleton (CHE) system is being dominated by the human nerve center, which give rise to correspondingly physical responses [8,9]. In order to exploit the interaction as a control input, the estimating torques from EMG signals called virtual torques along with regulated impedances were applied to the design of control laws [2,4]. Also, the measured interaction torques based on EMG were also fed into the force control law in [10]. In an effort to provide an alternative to the use of EMG sensors, Aguirre-Ollinger et al. [11] proposed a novel active-impedance control method that directly takes the information about the measured active torque from a human to produce a virtual adjustment of the mechanical impedances of the human limbs. However, obtaining accurate RPIT is not straightforward. An inverse dynamic model was used in [3] to isolate the human's active muscle force from passive effects, gravitation and inertia of the human-robot system.

With another approach, Kazerooni and his team developed robotic exoskeletons called the Berkeley Lower Extremity Exoskeleton (BLEEX) system [1,8] that can strengthen a users lower limb through a novel control method called Sensitivity Amplification Control (SAC). This control method added robustness to the system and minimized the use of sensory information from human-exoskeleton interaction. As a tradeoff, the key point to achieve the SAC control is that the dynamic model of the BLEEX system has to be identified as well as possible with a large number of parameters. By making use of the passive

Figure 1 A prototype of lower exoskeleton for human enhancement in PRMI.

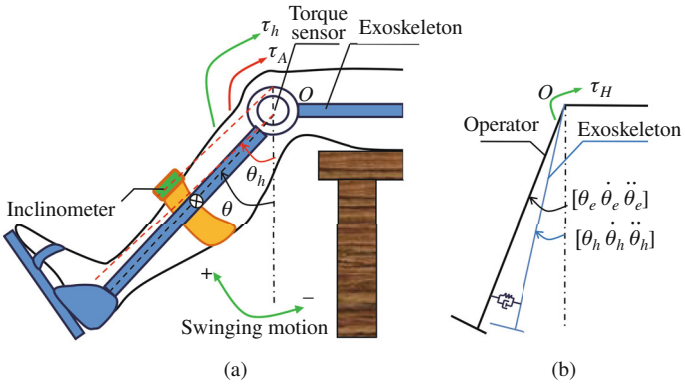

Figure 2 (a) A single DOF exoskeleton interacting with the operator's lower thigh during swinging motion; (b) master-slave model of the system.

dynamics of human walking, Herr et al. [9] proposed a concept of quasi-passive exoskeleton in which the quasi-passive elements of springs and variable dampers are exploited to improve the efficiency of exoskeleton devices. In this work, the strategy for finding the elastic structures that closely mimic the human musculoskeletal leg architecture is the main barrier to create a highly functional leg exoskeleton. Moreover, the implementation of the spring-damper mechanism on hardware configuration is essentially less flexible and efficient than on software. Similarly, to prove the effectiveness of control methods, spring-damper human-robot interaction models has been frequently used [3,5,6]. Because these models are not significantly convincing bringing back the effects of RPIT on the control performance, describing the RPIT is one of the main research questions in the lower exoskeletal robotic field.

3 Description

According to bio-mechanical studies of human behavior [12], the human walking gait cycle is divided into a number of distinct phases. For a single leg, it can be split into two phases: a load support stance phase and an unloaded swing phase. Here, the swing leg is subjected to large motions with high bandwidths contrary to the stance leg. For the coupled human-exoskeleton system, to capture higher order nonlinearities present in the RPIT, the dynamic behavior of the leg in swinging mode will be investigated, in which a single degree of freedom (DOF) platform will be studied. Since the operator's swing leg coupled with the exoskeleton is regarded as an n DOF multi-link pendulum, it is appropriate to consider the interaction resulting from the operator on one of these links at the knee joint.

3.1 Model of the combined human-exoskeleton system

The single DOF platform was set up as shown in Figure 2(a). In the platform, an operator's lower thigh fits closely to the 1-DOF exoskeleton when the operator swings his/her lower thigh according to a predefined motion. With this configuration, the exoskeleton including the human leg is assumed to be a rigid link pivoting about the knee joint, which is powered by a DC servo motor. The actuator torque τ_A about the pivot point O is produced by this DC motor. Besides, the total equivalent torque associated with the interaction forces from the operator on the exoskeleton is represented as the torque τ_H about the point O. The dynamic equation of the operator's shank including the lower exoskeleton can be represented as:

$$(I_E+I_H)\frac{\mathrm{d}^2\theta_e(t)}{\mathrm{d}t^2}+(D_E+D_H)\frac{\mathrm{d}\theta_e(t)}{\mathrm{d}t}+(M_E g l_E+M_H g l_H)\sin\theta_e(t)+C_a\mathrm{sign}\left(\frac{\mathrm{d}\theta_e(t)}{\mathrm{d}t}\right)=\tau_A(t)+\tau_H(t), \quad (1)$$

where I, D, M, and l represent inertial moment, viscous friction coefficient, lower thigh mass, and length, respectively, of the human subject (index H) and the exoskeleton (index E), C_a is Coulomb friction coefficient around the knee joint of the robot. A master-slave model of the system is depicted in Figure 2(b)

Table 1 Nonlinear mapping models of the resulting interaction torque from human. The coefficients M, B, K are exemplified as time varying ones

Case	Mapping model	Example
f_1	$\tau_{\text{int}} = f(\theta_h, \theta_e)$	$\tau_{\text{int}} = K(\theta_h - \theta_e)$
f_2	$\tau_{\text{int}} = f(\theta_h, \theta_e, \dot{\theta}_e, \ddot{\theta}_e)$	$\tau_{\text{int}} = M\ddot{\theta}_e + B\dot{\theta}_e + K(\theta_h - \theta_e)$
f_3	$\tau_{\text{int}} = f(\theta_h, \dot{\theta}_h, \theta_e, \dot{\theta}_e)$	$\tau_{\text{int}} = B(\dot{\theta}_h - \dot{\theta}_e) + K(\theta_h - \theta_e)$
f_4	$\tau_{\text{int}} = f(\theta_h, \dot{\theta}_h, \ddot{\theta}_h, \theta_e, \dot{\theta}_e, \ddot{\theta}_e)$	$\tau_{\text{int}} = M(\ddot{\theta}_h - \ddot{\theta}_e) + B(\dot{\theta}_h - \dot{\theta}_e) + K(\theta_h - \theta_e)$

in which the terms $(\theta_h, \dot{\theta}_h, \ddot{\theta}_h)$ denote the angular position, velocity and acceleration of the operator and $(\theta_e, \dot{\theta}_e, \ddot{\theta}_e)$ denote those of the exoskeleton with respect to vertical axis, respectively. Due to the functionality of human performance enhancement, the operator's knee joint angle is the master tracking trajectory with respect to the exoskeleton during motion.

3.2 Representation of the interaction resulting from the human

The remaining issue is how the characteristics of interaction environment from the human is described by the torque τ_H. In general, the RPIT τ_H equals the sum of the active torque τ_{act} from the human (muscle torque) and the torque τ_{int} modeled by a function of dynamic factors representing human-robot configuration during motion:

$$\tau_H(t) = \tau_{\text{act}} + \tau_{\text{int}}. \tag{2}$$

Here, the active torque τ_{act} that is dominated by the human central nervous system can be regarded as the impact torque at some instants. In the absence of this impact torque, the closest relation between the torque τ_H and the dynamic factors $(\theta_h, \dot{\theta}_h, \ddot{\theta}_h, \theta_e, \dot{\theta}_e, \ddot{\theta}_e)$ is found in the underlying interpretation of the regression technique. In early research, the representation of environment-robot interaction has been developed with numerous models of geometric constraints and dynamic factors [13]. From these models proposed in literature, the most typical possibilities will be herein considered as shown in Table 1. Let us discuss them.

Any interaction environment can also be expressed by a generalized model as f_4 [14]. Besides, it can be represented by a lower order model as f_3 when the robot is pushed or pulled by a human [15]. However, in order to validate control systems with the most vulnerable effect of the interaction, it can be described as the nonlinear function of the position deviation without damping f_1 [5,6]. A compliant work environment modeled as f_2 has been also exploited in many studies of the robot-environment interaction [16]. This work will cover all these cases as reported in [17].

In general, the determination of the structure and parameter of the nonlinear mapping (function) $f(\cdot)$ is not straightforward in the presence of strong nonlinearities and unpredictable human effects. Without loss of generality, these interaction torques are herein considered in two scenarios: (1) The exoskeleton naturally works to follow the operator's motion without control of the robot. (2) The exoskeleton constrainedly works for the tracking task with a simple master-slave controller. Since the goal of this study is not to control the robot, a position PD control with gravity compensation is chosen. On the other hand, the RPIT also depends on the property of each operator during locomotion. Hence, we will conduct experiments with three various operators, named operators A, B, and C, to generalize the findings. These experiments will be described in detail in the following sessions.

4 Supervised learning with nonparametric regression techniques

4.1 Statistical learning of nonlinear mapping of the RPIT

As discussed above, structure and parameter of the RPIT are hard to define explicitly. Therefore, supervised learning techniques are particularly suited for this kind of regression problems. In this paper, nonparametric regression methods were used to learn the mapping that describes the relationship from

the dynamic factors to the interaction. Among them, Gaussian Process Regression [18] is currently the standard global method with competitive performance but it has a high computation cost. Alternatively, Locally Weighted Projection Regression [19] was chosen as a representative of the local method that provide the ability of incremental robust learning and fast computation. This study comes with both the learning methods to select and compare the most appropriate models of the RPIT.

4.2 Gaussian Process Regression (GPR)

GPR is a regression method based on the Gaussian model that is fully specified by its mean function and covariance function [18]. From the weight-space view, a standard Gaussian model is given by the linear model for regression estimation:

$$f(x) = \psi(x)^{\mathrm{T}} w, \quad y = f(x) + \epsilon, \tag{3}$$

where x is the input vector, w is the weight vector, and ϵ is additive noise that follows an independent Gaussian distribution with zero mean and variance σ_n. The kernel function $\psi(\cdot)$ is to transform the input x into a space of higher order called feature space. With the linear approach in (3), the regression problem can be dealt with using various kernel functions, such as Gaussian kernel and others discussed in [18]. The probability density of the observed output y, called likelihood, with the given parameters $\psi(x)$ and w can be written as:

$$p(y|\Psi, w) \propto \mathrm{e}^{-\frac{|y-\Psi^{\mathrm{T}} w|^2}{2\sigma_n^2}} = N(\Psi^{\mathrm{T}} w, \sigma_n^2 I), \tag{4}$$

where the vectors y and w are target and weight ones, respectively, the matrix Ψ denotes the aggregation of columns $\psi(x)$ for all cases in the training set. Furthermore, the weights are assumed as Gaussian distributed with zero mean and variance Σ_p [18]. The probability density of w called prior is given by:

$$p(w) \propto \mathrm{e}^{-\frac{1}{2} w^{\mathrm{T}} \Sigma_p^{-1} w} = N(0, \Sigma_p). \tag{5}$$

The probability density of the weights, called posterior, given inputs, and targets is proportional to the product of likelihood and prior based on Bayes' rule:

$$p(w|\Psi, y) \propto \mathrm{e}^{-\frac{1}{2}(w-v)^{\mathrm{T}} A (w-v)} = N(v, A^{-1}), \tag{6}$$

where $A = \sigma_n^{-2} \Psi \Psi^{\mathrm{T}} + \Sigma_p^{-1}$ and $v = \sigma_n^{-2} A^{-1} \Psi y$. In order to predict at a new input x_p, the average of the outputs of all linear models are additionally weighted by their posterior. Thus, the predicted mean $\bar{f}_p$ and predicted variance V_p for a prediction $f(x_p)$ can be given as follow [18]

$$\bar{f}_p = k_p^{\mathrm{T}} (K + \sigma_n^2 I)^{-1} y = k_p^{\mathrm{T}} \xi, \quad V_p = k(x_p, x_p) - k_p^{\mathrm{T}} (K + \sigma_n^2 I)^{-1} k_p, \tag{7}$$

where $k_p = \psi_p^{\mathrm{T}} \Sigma_p \Psi$, $k(x_p, x_p) = \psi_p^{\mathrm{T}} \Sigma_p \psi_p$ and $K = \Psi^{\mathrm{T}} \Sigma_p \Psi$. It can be seen from (7) that the predicted value for a new observed input and the corresponding uncertainty of prediction are obtained by $\bar{f}_p$ and V_p, respectively. Furthermore, the prediction vector ξ that is computed for every training point influences prediction behavior globally, hence GPR is a global method.

4.3 Locally Weighted Projection Regression (LWPR)

LWPR is an incremental version of the locally weighted regression (LWR) algorithm [20] with automatic structure adaptation and lower computational cost. An LWPR model consists of a set of local linear models that come paired with a kernel that defines the area of validity of the local model. For a given input x, a weighting $\omega_k(x)$ is determined by the kernel of the kth local model while the local linear model predicts an output $\psi_k(x)$. The combined prediction of LWPR is calculated by the weighted average of N individual predictions:

$$\hat{y}(x) = \frac{\sum_{k=1}^{N} \omega_k(x) \psi_k(x)}{\sum_{k=1}^{N} \omega_k(x)}, \tag{8}$$

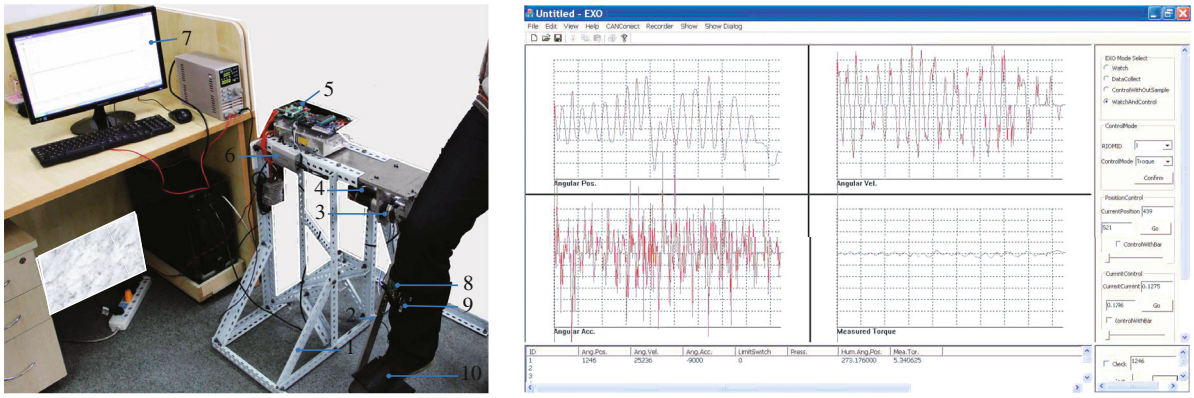

(a) (b)

Figure 3 (a) Experimental platform and implementation of experimental sessions for subject C; (b) designed interface for data visualization and collection. 1: Frame, 2: Exoskeleton arm, 3: Custom-built torque sensor, 4: Maxon DC motor and reducer, 5: Elmo driver and STM32F Microcontroller, 6: CAN-bus module, 7: PC and interface, 8: Custom-built inclinometer, 9: Accelerometer, 10: Bracket.

with $\psi_k(x) = \bar{x}_k^{\mathrm{T}}\widehat{\theta}_k$ and $\bar{x}_k = [(x - c_k)^{\mathrm{T}}, 1]^{\mathrm{T}}$. Here $\hat{\theta}_k$ contains the regression parameters and c_k is the center of the kth linear model. The region in which a linear model is valid is called the receptive field (RF). It is usually characterized by a Gaussian kernel:

$$\omega_k(x) = \exp\left(-\frac{1}{2}(x - c_k)^{\mathrm{T}} D_k (x - c_k)\right), \tag{9}$$

where D_k is a positive definite matrix called distance metric. The main goal of the learning process is to adjust D_k and $\hat{\theta}_k$ so that the error between the predicted values and the targets is minimal. For learning the linear models $\psi_k(x)$, the regression parameter $\hat{\theta}_k$ is calculated by an online formulation of weighted partial least squares (PLS) regression [21], instead of recursive least square (RLS) presented in [22]. The distance matrix D_k determines the locality of each local model that can be learned individually by the stochastic gradient descent. Based on a given cost function J_k, distance metric D_k is updated as the following rule:

$$D_k = M_k^{\mathrm{T}} M_k, \quad \text{with } M_k^{n+1} = M_k^n - \alpha \frac{\partial J_k}{\partial M_k}, \tag{10}$$

where M_k is an upper triangular matrix that ensures D_k to be positive. Minimizing the penalized weighted mean squared error expressed in J_k, the distance metric D_k can be obtained [23]. The number of receptive fields is updated automatically. If a training data point x does not activate any RF by more than a constant ω_{gen} a new RF is created centered at x. Parameter ω_{gen} is a tunable one called meta-parameter. Besides, there are several other parameters related to the convergence and approximation error of the algorithm that need to be tuned manually during learning. Please refer [21,23,24] for more details on implementing LWPR and tuning the parameters.

5 Experimental results and analysis

5.1 Experimental setup

A 1-DOF exoskeleton platform has been designed and built for performing the experiments with various knee flexion/extension sessions. Figure 3(a) shows the mechanical design and the hardware configuration of the exoskeleton assisting the operators. The sessions employed on this platform use the pendular motion of the lower thigh as a representative scaled-down model of the swing leg in walking cycles. Whereby, the effect of dynamic factors on the resulting interaction torque has been evaluated. As shown in Figure 3, the assembly of the exoskeleton platform typically consists of a stationary frame, a DC servo motor with a customized harmonic gearbox, and an exoskeleton arm.

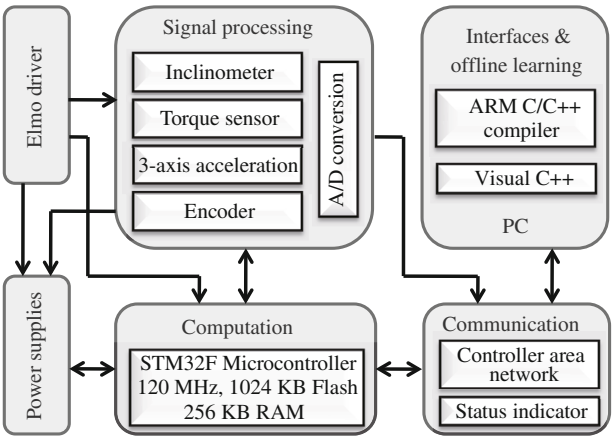

Figure 4 Diagram of the distributed embedded system.

The motor has an incremental optical encoder (an HP optical encoder HEDS) on its shaft with a resolution of 2000 counts per revolution that allows the measurement of the knee angle of the exoskeleton arm. The exoskeleton arm is made of aluminum with a customized design to reduce its weight and inertia. A custom-built inclinometer is attached to the operator's shank to measure the angular position of his/her shank relative to gravity. We designed it using a L3G4200D three-axis angular rate sensor and an ADXL345 three-axis accelerometer with high resolution (13 bit). Besides, a custom-built torque sensor was used to measure the active torque from the human (the interaction torque). It is located between the motor's shaft and the pivoting arm. To avoid the error resulting from using numerical differentiation method for the calculation of angular accelerations, digital inertial measurement units were used on both the human and exoskeleton to attenuate uncertainties occurred in the motion data.

During development of the exoskeleton-human system in PRMI laboratory, we designed an embedded control system that enables the main controller to interchange information with distributed sensors favorably, increase the ability of integration, and ensure real-time control performance. For one DOF experimental platform, the designed hardware configuration was utilized as part of the whole distributed embedded system in the project. The hardware consists of a 120 MHz STM32F microcontroller as the main computational module with respect to this platform, a personal computer (PC) for developing a graphical user interface and executing the offline learning procedure, and an Elmo's digital servo drive for driving the DC motor. The microcontroller is responsible for providing the sensory inputs to the PC, sending appropriately computed control signals to the driver and vice versa. It communicates with the PC via Controller Area Network (CAN1) to provide an understandable and consistent behavior and comfortable data visualization. The Elmo drive also communicates with the controller via CAN network (CAN2). Figure 4 represents the general embedded system framework used in the platform. Since the experiments are related to human motion, the safety feature in the design of both the mechanical structure and the controller has been considered.

5.2 Experiments without control

Experiments were independently performed with three selected subjects. They are healthy people whose weights were 73 kg (subject A), 65.5 kg (subject B), and 69 kg (subject C). These operators were instructed to swing their shank to follow bounded sinusoidal trajectories. In order to collect data, the operators wore the exoskeleton at the foot bracket and, simultaneously fixed the inclinometer and the acceleration sensor properly at their lower thigh. As discussed above, each collected data set consists of six inputs $\Phi = (\theta_h, \dot{\theta}_h, \ddot{\theta}_h, \theta_e, \dot{\theta}_e, \ddot{\theta}_e)$ and one output $[\tau_{\text{int}}]$. We designed a user interface to display and store the collected data for each operator on the PC as seen in Figure 3(b). For each subject, ten trials of training and prediction were performed so that the relationship can be evaluated under the same conditions (before and after learning). For example, only the data gathered by the swinging motions

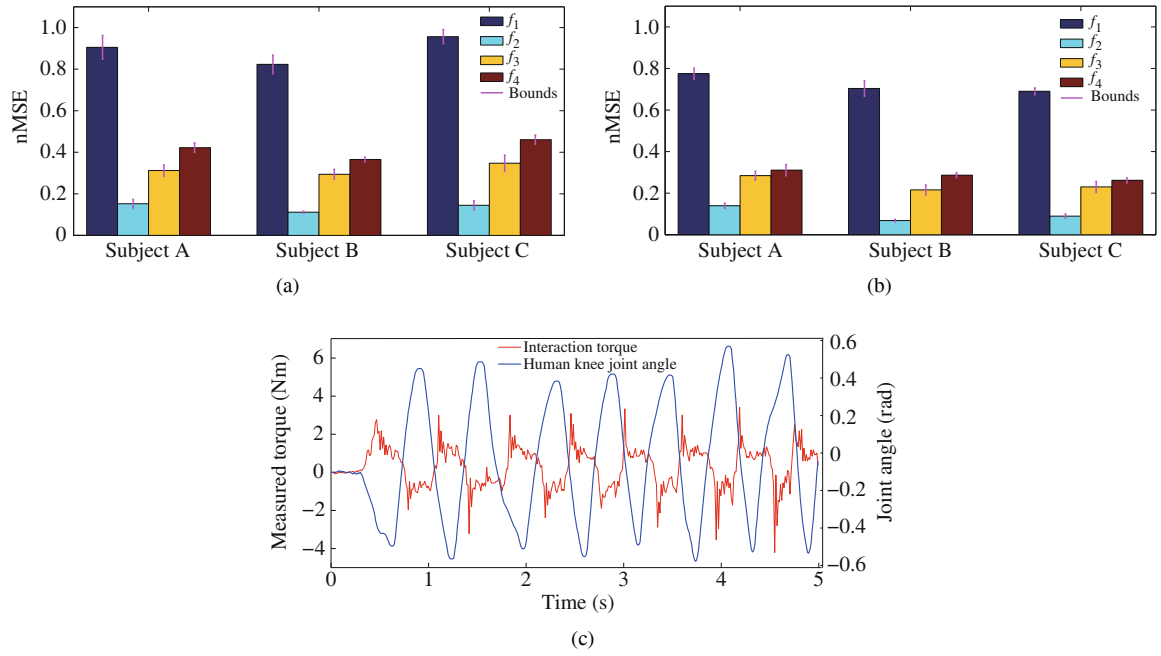

Figure 5 (a) A sample for training without control. Prediction error of the interaction torque on collected data without control using LWPR (b) and GPR (c). Here, the measured frequency of motion for training is 1.46 Hz and for prediction is 1.35 Hz.

with frequencies typically between 1.2 Hz and 1.5 Hz has been stored for training and then the subject would be instructed to swing his leg with similar frequencies for prediction and testing. Figure 5(a) shows a training sample collected when the operator B swung his leg with measured frequency of around 1.46 Hz. For clarity, the data of measured torque has not been smoothed or filtered.

After training and testing procedure, Figure 5 (b) and (c) show the averaged prediction error of the resulting interaction torque computed by the average of the normalized mean square error (nMSE) with respect to each mapping model over the ten trials. In Figure 5(b) we can see that nMSE reaches the lowest value of around 0.10 to 0.15 with the second case of mapping models (f_2) using LWPR. Similar results were achieved using GPR as shown in Figure 5(c), with lower nMSE in almost all cases. This demonstrates that the ability of generalization of GPR is better than LWPR when the latter algorithm is affected by many manual setting parameters. Here, these parameters such as metric D or coefficient ω_{gen} were tuned experimentally from comparing the performance of a set of resulting interaction torques to find the best value corresponding to the minimal prediction error. Among all the considered cases, the mapping model f_1 is apparently the most inappropriate as this model provides the highest prediction error, around 0.73 to 0.91. The two remaining cases, f_3 and f_4, bring acceptable models for predicting the interaction when nMSE drops to a relatively small range of [0.32 0.55]. However, as seen in the above results, the mapping model f_2 is still the best choice with the convergence of learning algorithm as well as the prediction error. The nMSE after learning with the model f_1 is decreased by about 40%–55% compared to that with the models f_3 and f_4, and decreased over 80%–90% compared to that with f_1 (on the same operator and learning method). Figure 6(a) also clarifies the above discussion through an example of prediction procedure with a sampled data set using LWPR. Here, the case of the prediction with f_4 is not shown so that the differences in prediction are readily apparent.

5.3 Experiments with a simple master-slave control

Similar to the above experiments, the subjects A–C attached in the exoskeleton were also instructed to perform the swinging sessions but using a PD master-slave control of the robot. In fact, it is not sufficiently suitable to use this controller in swinging motion since the robot is subjected to large motions and therefore needs high bandwidth. In this case, it is easy to result in a chattering phenomenon and

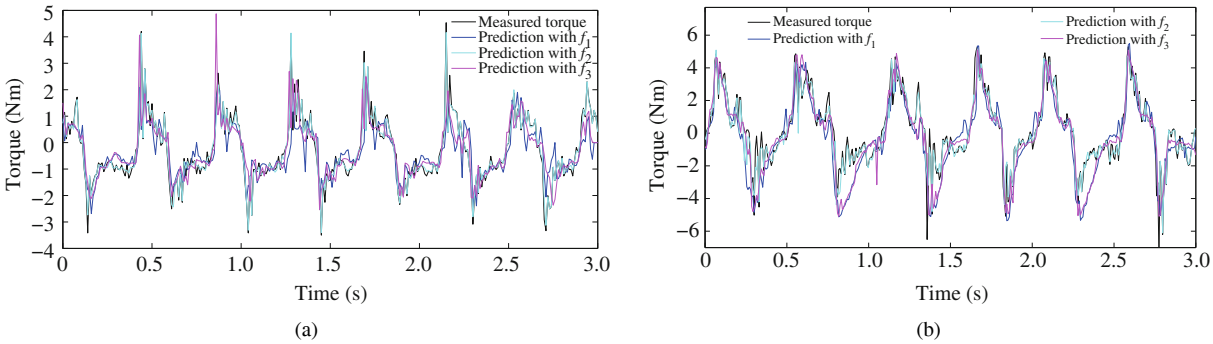

Figure 6 Example of prediction on trained data without control (a) and with master-slave control (b) using LWPR.

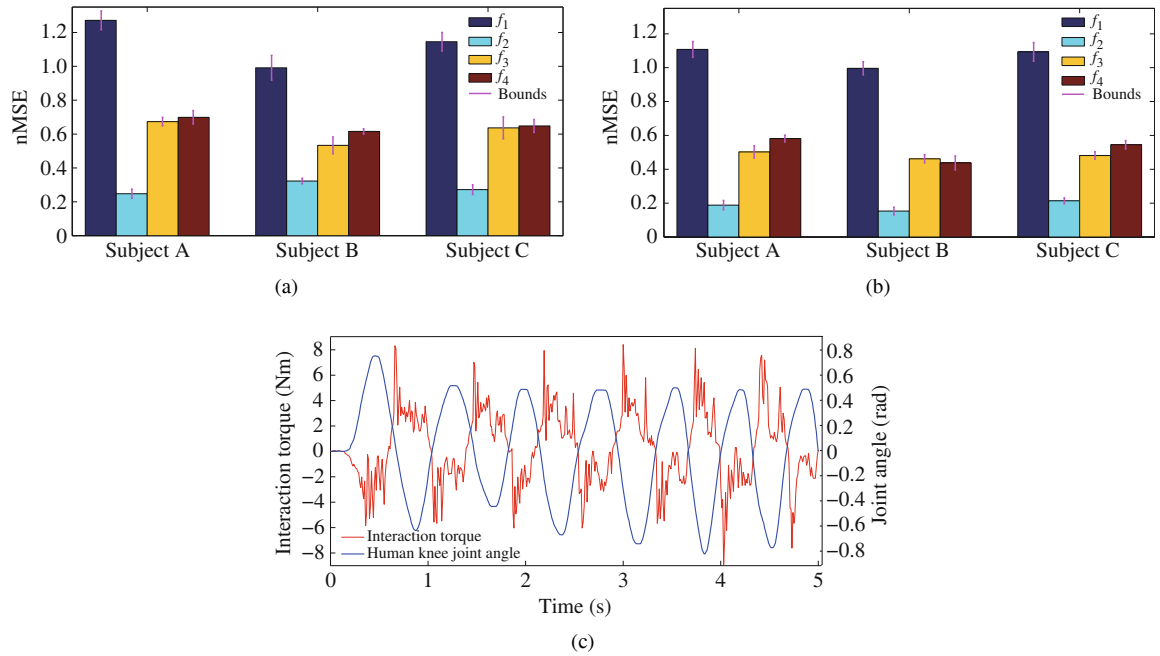

Figure 7 (a) A sample for training with control. Prediction error of the interaction torque on collected data with master-slave PD control using LWPR (b) and GPR (c). Here, the measured frequency of motion for training is 1.22 Hz and for prediction is 1.08 Hz.

large errors in tracking control. This is demonstrated through an example in Figure 6 when the collected interaction torque is significantly larger and more irregular than the case without control. Nevertheless, we accept this choice as a tradeoff for collecting data and capturing the interaction naturally. For the master-slave control, the controller takes the error of the knee joint angles of the master (operator) and the slave (exoskeleton) as input. If we bind the two together with rigid connections, the control output goes to zero. That means it would impede the motion of the master. Consequently, the connection is only at the foot in our experimental setup, and other remaining positions, e.g. around the knee joint, are set to be free. With this connection, the master-slave control of the exoskeleton is obviously guaranteed, but without good performance.

Here, the swinging motions with frequencies belonging to 0.9–1.3 Hz were carried out and the experimental process was similar to the one without control. Figure 7(a) typically shows one of the training samples that was collected with a measured frequency of around 1.25 Hz. We can see in Figure 7(b), the comparing prediction quality using mapping model f_2 to other ones, nMSE of model f_2 is significantly smaller (around 0.22 to 0.31). Similar to the case without control, the error using GPR is slightly lower compared to LWPR as seen in Figure 7(c) (about 10%–20%). Comparing the results in Figure 5 and Figure 7, it can be seen that a close result was generally achieved using both LWPR and GPR method, regardless of whether the exoskeleton is controlled or not. The fundamental difference between the results

lies in the fact that the learning accuracy of GPR is slightly higher compared to LWPR and the larger errors emerge while the exoskeleton works under constrain as it is controlled by the operator.

6 Control applications based on the learned models

In this section, we briefly present the control applications of the learned models of the RPIT in our published researches. Please see [25] for more details on evaluations and results of these applications. The goal of this section is to point out the advantages of the above learning results.

6.1 Variable impedance control with the learned interaction model

Impedance control, firstly proposed by Hogan [26], is one of the most popular methods for controlling robotic manipulators in contact with external environments, especially for applying to human-assisting robotic exoskeletons. By implementing in various forms, the effectiveness of the impedance control for the robotic lower exoskeletons has been demonstrated [3,27] through the regulation of the characteristics of the interaction forces resulting from the human and motion control. The main work involved in the design of an impedance control for a robotic exoskeleton is to achieve an appropriate structure and a desired set of impedance parameters so that the dynamics of the robot-human interaction behavior can get the expected response.

As highlighted by the above learning results, the structure of the impedance model describing the relationship between the desired impedance torque τ_{imp} and the deviation $\Delta\theta$ between the knee joint angles of the operator and the exoskeleton should be selected as a general form [17] or the following form:

$$\tau_{\text{imp}}(s) = Js^2\Delta\theta(s) + Ds\theta_e(s) + K\theta_e(s), \tag{11}$$

where, J, D, and K are the inertial, damping and stiffness components, respectively. The term $\Delta\theta(s) = \theta_h(s) - \theta_e(s)$ and $\theta_h(s)$ represents the operator's knee angle. The regulation of the inertial, stiffness, and viscous coefficients of the impedance controller depends on environmental tasks. Since human physical property playing the role of the interaction environment is different from person to person and is dominated by the dynamic factors of the CHE system during motion, the relation in (11) is explicitly time varying nonlinear. This means that traditional impedance control methods frequently face difficulty in finding the desired impedance parameters. Therefore, these impedance coefficients should be dynamic and predefined to adapt to these differences. In our research [25], we have proposed a newly fuzzy-based impedance control strategy that provides the exoskeleton with the ability to adapt to various motion speeds of a human operator and to reduce the resulting physical interaction between the operator and the exoskeleton. That means, after having a suitable structure of impedance model from the above results, we also need an intelligent strategy to regulate the impedance parameters. As an example, a fuzzy-based impedance control strategy depicted in Figure 8 was adopted in [25]. In this strategy, the inertial and stiffness parameters are empirically chosen in advance while the viscous parameter is inferred by a fuzzy-based regulator. The analyses, design, and experimental validations of the strategy were also reported in the literature.

Our results indicate that the proposed control along with the corresponding learned impedance structure have provided the exoskeleton with the ability to adapt to various ranges of motion speed and improve control performance of the physical human-exoskeleton interaction.

6.2 Partitioned control with learned dynamics-interaction model

Inspired by this study, we have developed a control algorithm that takes advantage of the incremental learning technique to improve the control of the lower exoskeleton and to compensate the RPIT[1)]. As depicted in Figure 9(b), the dynamics of the combined human-exoskeleton system along with the corresponding resulting interaction torques are learned based on nonparametric regression technique and then

1) Tran H-T, Cheng H, Duong M-K. Learning dynamic model of a lower exoskeleton interacting with human for partitioned control. Int J Adv Rob Syst, 2014, submitted.

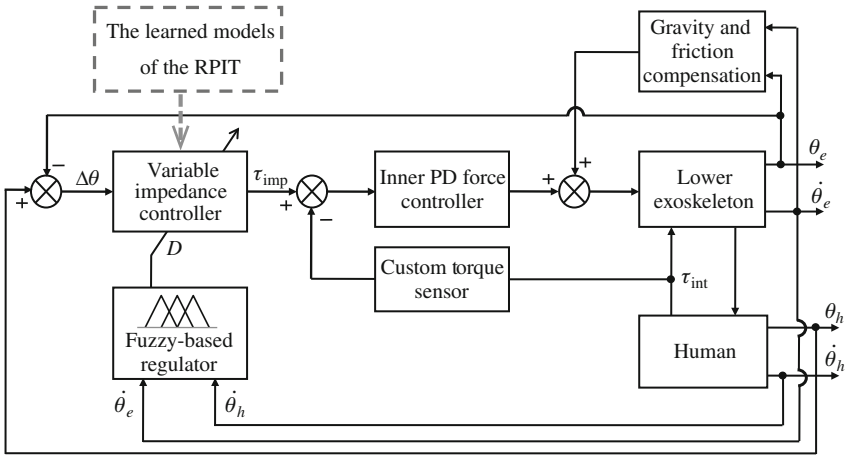

Figure 8 Principle of the fuzzy-based regulated impedance control for the lower exoskeleton interacting with human.

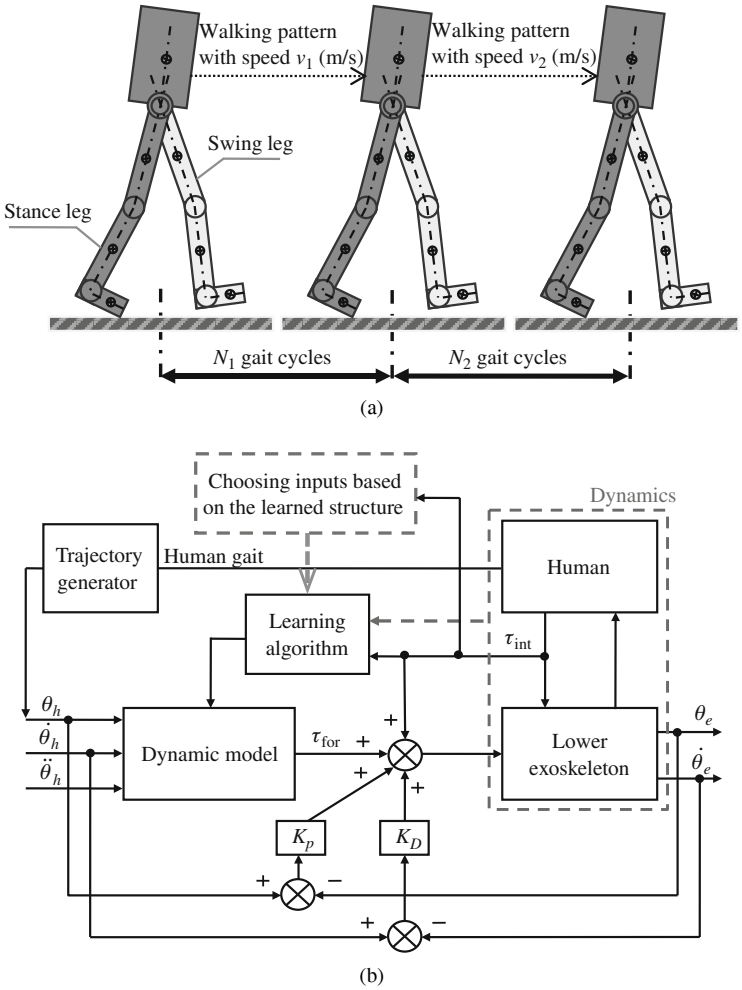

Figure 9 (a) Duration of data collection for learning and control: N_1 gait cycles for collecting data using a simple master-slave position control; N_2 gait cycles driven by proposed control algorithm; (b) principle of partitioned nonlinear control applied to lower exoskeleton with interaction-dynamics learning.

incorporated into the partitioned control scheme. By doing so, the exoskeleton is driven flexibly and compliantly following the operator's locomotion. This is because the partitioned control will compensate both dynamics nonlinearities and the resulting interaction torques using the model being learnt. Regard-

ing the data collection process for learning, the operator-exoskeleton system is controlled by a simple master-slave PD controller (with gravity compensation) so that the exoskeleton can track the operator's movement in the first several gait cycles as seen in Figure 9(a).

For design of the learning strategy, one of the key points to be considered is the most relevant dynamic inputs that would affect the RPIT. In other words, the structure of nonlinear mapping model $f(\cdot)$ of the RPIT and dynamic factors should be determined in advance. With the results shown in Section 5, the proposed control algorithm has been efficiently implemented online using the learning input set of $(\theta_h, \theta_e, \dot{\theta}_e, \ddot{\theta}_e)$. It is well known that by using the approach of dynamic model learning, we can simultaneously deal with many obstacles in lower exoskeleton control.

Satisfactory results of the simulation and experiments on a typical example have been achieved[1)], with the convergence of the learning algorithm and the significant reduction of the interaction torque. Compared to other conventional control methods, the proposed method provided better performances, such as the least human-robot tracking error or the lowest human-exoskeleton interaction, and thus the exoskeleton could assist/support the operator without discomfort. Nevertheless, we have faced some major drawbacks during implementation of this investigation. For example, the human operator has to move with difficulties in the first motions as the simple master-slave controller partly satisfy the requirement of collecting data. Besides, the algorithm is suitable only for a specified range of operation during locomotion. Although these issues become the major drawbacks in this study, we have accepted them as unavoidable.

7 Conclusion and future work

In this paper, we have carried out experiments to find out the relationship between the resulting interaction torque and the dynamic factors in the collaboration of the human-exoskeleton system using LWPR and GPR methods. Here, nonlinear mapping models were competitively studied to evaluate the extent of projection in the context that the system is under control or without control. During implementation of this investigation, we faced several drawbacks. For example, the manual tuning for parameters of the learning algorithms gives rise to tediousness for designers by trial-and-error, or the difficulties are faced since the human operator has to move with the simple master-slave controller of the exoskeleton. However, the collected data was sufficiently reliable and the learning algorithms converged in almost all cases. We have taken advantage of these results to apply for a fuzzy-based variable impedance control and an advanced partitioned control strategy.

Our results indicate that the nonlinear mapping model of the operator's angular position, and the exoskeleton's angular position, velocity, and acceleration is the most appropriate to represent the resulting interaction from the human. This model (mapping model f_2 in Table 1) provides potential applications in the field of physical human-robot interaction. Our next step is to utilize the findings to develop more intelligent control applications with the ability to adapt to various dynamics of human operators, predict and also compensate the physical interaction between the operator and the exoskeleton.

Acknowledgements

This work was supported by the grant of National Natural Science Foundation of China (Grant No. 61273256). The authors would like to express our sincere appreciation to our fellows at PRMI laboratory for their contribution on the fabrication of the device.

References

1 Kazerooni H, Racine J L, Huang L, et al. On the control of the Berkeley Lower Extremity Exoskeleton (BLEEX). In: Proceedings of the IEEE International Conference on Robotics and Automation, Barcelona, 2005. 4353–4360

2 Lee S, Sankai Y. Power assist control for walking aid with HAL-3 based on EMG and impedance adjustment around knee joint. In: Proceedings of the IEEE International Conference on Intellegent Robots and Systems, Lausanne, 2002. 1499–1504

3 Riener R, Lünenburger L, Jezernik S, et al. Patient-cooperative strategies for robot-aided treadmill training: first experimental results. IEEE Trans Neural Sys Rehabil Eng, 2005, 13: 380–394

4 Hayashi T, Kawamoto H, Sankai Y. Control method of robot suit HAL working as operator's muscle using biological and dynamical information. In: Proceedings of the IEEE International Conference on IROS, Center Edmont, Alberta, 2005. 3063–3068

5 Gomes M A, Silveira G L M, Siqueirav A A G. Gait pattern adaptation for a active lower-limb orthosis based on neural networks. Adv Robot, 2012, 25: 1903–1925

6 Racine J L. Control of a Lower Extremity Exoskeleton for Human Performance Amplification. Dissertation for the Doctoral Degree. University of California, Berkeley, 2003

7 Sigaud O, Salaün C, Padois V. On-line regression algorithms for learning mechanical models of robots: a survey. Robot Auton Syst, 2011, 59: 1115–1129

8 Kazerooni H, Chu A, Steger R. That which does not stabilize, will only make us stronger. Int J Robot Res, 2007, 26: 75–89

9 Walsh C J, Endo K, Herr H. A quasi-passive leg exoskeleton for load-carrying augmentation. Int J Hum Robot, 2007, 4: 487–506

10 Zabaletal H, Bureau M, Eizmendi G, et al. Exoskeleton design for functional rehabilitation in patients with neurological disorders and stroke. In: Proceedings of the IEEE 10th International Conference on Rehabilitation Robotics, Noordwijk, 2007. 112–118

11 Aguirre-Ollinger G, Colgate J E, Peshkin M A, et al. Active-impedance control of a lower-limb assistive exoskeleton. In: Proceedings of the IEEE 10th International Conference on Rehabilitation Robotics, Noordwijk, 2007. 188–195

12 Winter D A. Biomechanics and Motor Control of Human Movement. 4th ed. New Jersey: Jonh Wiley and Sons Inc, 2009

13 Vukobratović M, Matijevic V, Potkonjak V. Control of robots with elastic joints interacting dynamic environment. J Int Robot Sys, 1998, 23: 87–100

14 Tsuji T, Tanaka Y. On-line learning of robot arm impedance using neural networks. Robot Auton Syst, 2005, 52: 257–271

15 Šabanović A, Ohnishi K. Motion Control Systems. John Wiley and Sons Inc, 2011

16 Tsuji T, Ito K, Morasso P G. Neural network learning of robot arm impedance in operational space. IEEE Trans Syst Man Cybern, 1996, 26: 290–298

17 Tran H-T, Cheng H, Duong M-K. Learning the relation of physical interaction to dynamic factors during human-exoskeleton collaboration. In: Proceedings of IEEE Conference on Multisensor Fusion and Information Integration, Beijing, 2014, in press

18 Rasmussen C E, Williams C K. Gaussian Processes for Machine Learning. Cambridge: MIT Press, 2006

19 Schaal S, Atkeson C G, Vijayakumar S. Scalable techniques from nonparametric statistics for real-time robot learning. Appl Intell, 2002, 17: 49–60

20 Atkeson C G, Moore A W, Schaal S. Locally weighted learning. Artif Intell Rev, 1997, 11: 11–73

21 Vijayakumar S, Schaal S. Locally weighted projection regression: an O(n) algorithm for incremental real time learning in high dimensional space. In: Proceeding of the 16th Conference on Machine Learning, San Francisco, 2000. 1076–1089

22 Nakanishi J, Farrell J A, Schaal S. Composite adaptive control with locally weighted statistical learning. Neural Netw, 2005, 18: 71–90

23 Vijayakumar S, D'Souza A, Schaal S. Incremental online learning in high dimensions. Neural Comput, 2005, 12: 2602–2634

24 Klanke S, Vijayakumar S, Schaal S. A library for locally weighted projection regression. J Mach Learn Res, 2008, 9: 623–626

25 Tran H-T, Cheng H, Duong M-K, et al. Fuzzy-based impedance regulation for control of the coupled human-exoskeleton system. In: Proceedings of the IEEE Conference on Robotics and Biomimetics, Bali, 2014, in press

26 Hogan N. Impedance control: an approach to manipulation. Part I, II, III. J Dyn Syst Meas Contr, 1985, 107: 1–24

27 Unluhisarcikli O, Pietrusinski M, Weinberg B, et al. Design and control of a robotic lower extremity exoskeleton for gait rehabilitation. In: Proceedings of the IEEE/RSJ International Conference on Intelligent Robots and Systems, San Francisco, 2011. 25–30